SLAC-PUB-14313

Single Dirac Cone Topological Surface State and Unusual Thermoelectric Property of compounds from a New Topological Insulator Family

Y. L. Chen,[1,2,3] Z. K. Liu,[1,2] J. G. Analytis,[1,2] J. -H. Chu,[1,2] H. J. Zhang,[1,2] B. H. Yan,[1,2] S. -K. Mo,[3] R. G. Moore,[1] D. H. Lu,[1] I. R. Fisher,[1,2] S. C. Zhang,[1,2] Z. Hussain,[3] and Z. -X. Shen[1,2]

[1]*Stanford Institute for Materials and Energy Sciences, SLAC National Accelerator Laboratory, 2575 Sand Hill Road, Menlo Park, California 94025*

[2]*Geballe Laboratory for Advanced Materials, Departments of Physics and Applied Physics, Stanford University, Stanford, California 94305*

[3]*Advanced Light Source, Lawrence Berkeley National Laboratory Berkeley California, 94720, USA*

(Dated: October 18, 2010)

Angle resolved photoemission spectroscopy (ARPES) study on $TlBiTe_2$ and $TlBiSe_2$ from a Thallium-based III-V-VI_2 ternary chalcogenides family revealed a single surface Dirac cone at the center of the Brillouin zone for both compounds. For $TlBiSe_2$, the large bulk gap ($\sim 200meV$) makes it a topological insulator with better mechanical properties than the previous binary 3D topological insualtor family. For $TlBiTe_2$, the observed negative bulk gap indicates it as a semi-metal, rather than a narrow gap semi-conductor as conventionally believed; this semi-metality naturally explains its mysteriously small thermoelectric figure of merit comparing to other compounds in the family. Finally, the unique band structures of $TlBiTe_2$ also suggests it as a candidate for topological superconductors.

PACS numbers: 71.18.+y, 71.20.-b, 73.20.-r, 73.23.-b

Topological insulators represent a new state of quantum matter with a bulk gap and odd number of relativistic Dirac fermions on the surface [1]. Since the discovery of two dimensional (2D) topological insulator in HgTe quantum well [2, 3] and subsequent in 3D materials (especially the single Dirac cone family Bi_2Te_3, Bi_2Se_3 and Sb_2Te_3)[4–6], topological insulators has grown as one of the most intensively studied fields in condensed matter physics [1–14]. Moreover, the massless Dirac fermions and the magnetism in topological insulators can further link them to relativity and high energy physics[15]. The fast development of topological insulators also inspires the study of other topological states such as topological superconductors[11–13, 16, 17], which has a pairing gap in the bulk and topologically protected surface state consisting of Majorana fermions[11]. Unlike Dirac fermions in topological insulators that can have the form of particles or holes, Majorana fermions are their own antiparticles[18]. The simplest 3D topological superconductor consists of a single Majorana cone on the surface, containing half the degree of freedom of the Dirac surface state of a single cone 3D topological insulator. This fractionalization of the degree of freedom introduces quantum non-locality and is essential to the topological quantum computing based on Majorana fermions[19].

In this work, we use ARPES to study the electronic structure of $TlBiTe_2$ and $TlBiSe_2$ from a recently proposed topological insulator family of Thallium-based ternary chalcogenides[14, 20]. Remarkably, a single Dirac cone centered at the point of surface Brillouin zone (BZ) is found in both materials; and the surface and bulk electronic structures measured by ARPES are in broad agreement with *ab initio* calculations. Furthermore, for the p-type $TlBiTe_2$, the experimental band structure reveals six leaf-like bulk pockets around the surface Dirac cone. Given that these bulk pockets are the only structure other than the Dirac cone on the Fermi-surface (FS), they provide a possible origin for the reported bulk superconductivity[21], which can further induce superconductivity to the surface state by proximity effect, making $TlBiTe_2$ a possible candidate for 3D topological superconductors. Another compound of the family, $TlBiSe_2$ has a simpler bulk structure around the Dirac cone at Γ with the Dirac point resides in the bulk energy

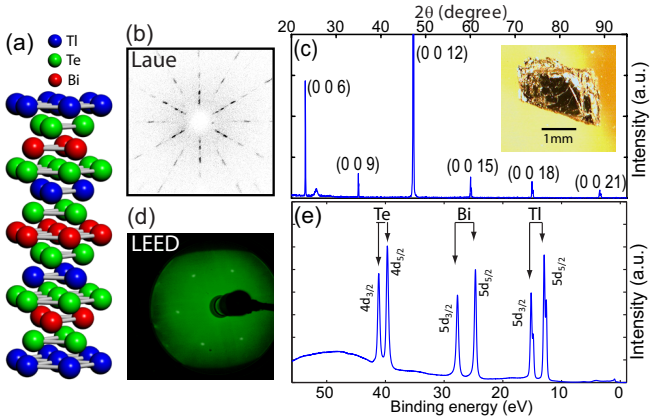

FIG. 1: (color) (a) Crystal structure of $TlBiTe_2$ with repeating -Tl-Te-Bi-Te- layers. (b,c) Laue and XRD characterizations show the high quality of the crystal. Inset in (c) shows a flat cleavage surface along (111) direction. (d) LEED pattern acquired after ARPES demonstrates clear diffraction spots without surface reconstruction. (e) Core level PES shows the d-shell electron peaks of all three compositional elements.

Work supported in part by US Department of Energy contract DE-AC02-76SF00515.

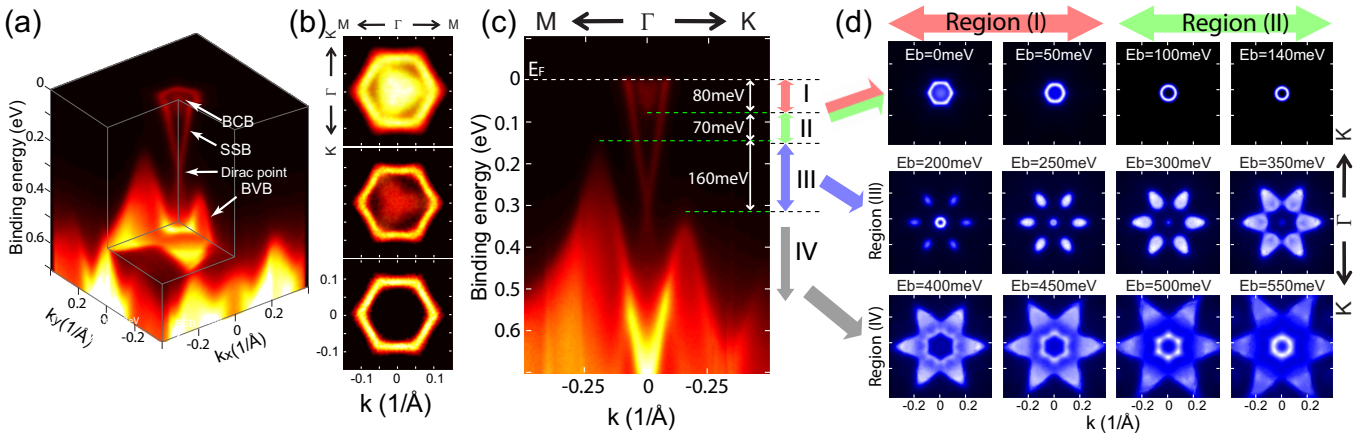

FIG. 2: (Color) (a) 3D band structure of $TlBiTe_2$, with the BCB, BVB, SSB and the Dirac point indicated. (b) FS maps (symmetrized according to the crystal symmetry) for 21, 23, and 25eV photons. (c) Dispersion along M-Γ-K direction. Four regions defined by characteristic energy positions are labeled as I, II, III, and IV. (d) Constant energy plots of the band structure from different regions defined in (c), showing the BCB FS inside SSB (region I), SSB only (region II), BVB outside SSB (region III) and all BVB (region IV).

gap (∼200meV), making it a large gap topological insulator similar to Bi_2Se_3[4], but with much better mechanical properties, as the covalence bonding between atomic layers in $TlBiSe_2$ are much stronger[14] than the van de Waals' force that bonds quintuple layer units of Bi_2Te_3 or Bi_2Se_3[4].

Interestingly, the ternary III-V-VI_2 family compounds are also known as good high-temperature themoelectric materials[22–27], and a long standing puzzle since 1960's has been the unusually low themoelectric figure of merit (ZT) of $TlBiTe_2$ ($ZT \sim 0.15$) due to its much smaller thermoelectric power S ($\sim 70\mu V/K$) [22, 24] comparing to that of other compounds ($ZT \sim 0.9, S \sim 200\mu V/K$)[25, 26] in the family. By observing a negative band gap in the band structure, we demonstrats that $TlBiTe_2$ is a semi-metal, contrast to a narrow-gap semiconductor as conventionally believed[23, 27], thus naturally explains its mysteriously small thermoelectric power, as will be discuss later in the paper.

The crystal structure of $TlBiTe_2$ is shown in Fig. 1, and the X-ray diffraction (XRD), Laue and Low energy electron diffraction (LEED) characterizations all show the high quality of the samples use for ARPES measurements.

The band structure of $TlBiTe_2$ around the BZ center is presented in Fig. 2, in which the 3D plot [Fig.2(a)] shows a clear Dirac cone centered at Γ-point surrounded by broad features from the bulk conduction (BCB) and bulk valence band (BVB). To confirm the surface nature of the Dirac cone, excitation photon energy dependent ARPES study [Fig. 2(b)] was performed. The non-varying shape of the outer hexagonal surface state band (SSB) FS under different photon energies indicates its 2D nature; while the shape and the existence of the BCB FS pocket inside changes dramatically due to its 3D nature with strong k_z dispersion.

Detailed band dispersions along two high symmetry directions (Γ-M and Γ-K) are illustrated in Fig. 2(c). The linear dispersion of the SSB clearly indicate a massless Dirac fermion with a velocity of $\sim 6.23\times10^5$ m/s (4.11eV·Å), about 1.5 times larger than the value in Bi_2Te_3[6]; and the broad features come from the bulk bands, among which an asymmetry of the BVB between the two directions can be seen. Based on the characteristic energy positions of the bulk band, we can divide the band structure into four regions [Fig. 2(c)] for discussion of different FS geometries [Fig. 2(d)]. From region I to III, the bulk contribution evolves from an n-type pocket inside (region I) the n-type SSB FS to six p-type leaf-like pockets outside (region III), with the bulk pockets disappear in region II; while in region IV, both the SSB pocket at the center and the surrounding leaf-like bulk pockets are p-type.

Besides having the single Dirac cone on the surface, $TlBiTe_2$ was also reported to superconduct when p-doped[21], with E_F of the corresponding density ($\sim 6\times10^{20}/\mathrm{cm}^3$) resides in region III (∼150meV below the bottom of BVB). From our measurements, the FS geometry in this doping region is characterized by a ring like SSB FS and six surrounding p-type bulk pockets [Fig. 3(a)], as clearly shown in region III of Fig. 2(d). A broad scan in $k-$space that covers four BZs [Fig. 3(b)] confirms that the FS structure shown in Fig. 3(a) is the only feature within each BZ. This leads to the natural conclusion that the bulk superconductivity of $p-$type $TlBiTe_2$ originates from the six leaf-like bulk pockets; and in the superconducting state, the surface state [the center FS pocket in Fig. 3(a,b)] can become superconducting due to the proximity effect induced by the bulk superconductivity. For such a superconductor, it has been proposed[11] that

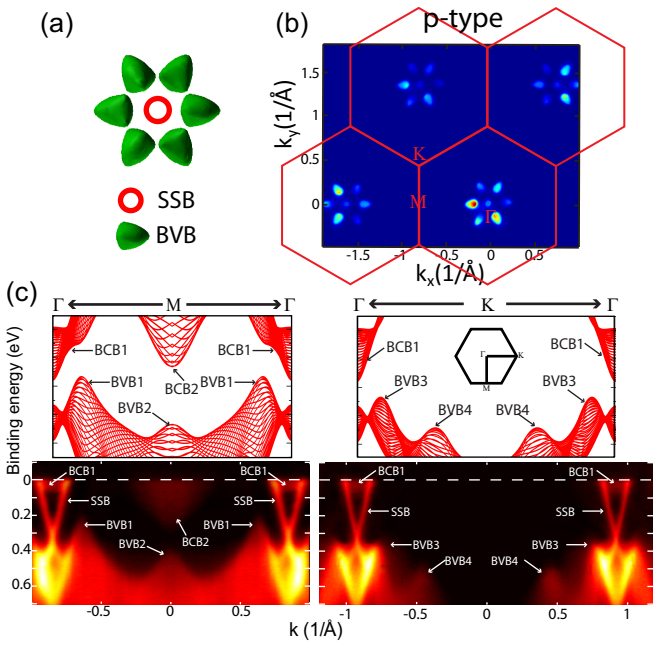

FIG. 3: (Color) (a)Typical FS geometry in region III as defined in Fig. 2. (b) Broad k-space scan shows no additional features besides the FS pockets illustrated in (a). High symmetry points Γ, M and K are marked; the uneven intensity at different BZs results from the matrix element effect. (c) Comparison between the *ab initio* calculation (top panels) and experimental band structures (bottom panels),with the prominent BCB, BVB and SSB features labeled.

each vortex line has two Majorana zero modes related by the time reversal symmetry, making it a candidate for the long sought after topological superconductors and suitable for the topological quantum computation[19]. However, the presence of superconductivity in $p-$type $TlBiTe_2$ requires further confirmation[28].

The band structures of $TlBiTe_2$ in larger energy and momentum scale are shown in Fig. 3(c). In general, the experimental dispersions along both directions agree well with the calculation, which reproduces each bulk feature of the measurement [Fig. 3(c)], except an importance difference, that the ARPES measurement [Fig. 3(c), bottom left panel] clearly shows a negative energy gap (∼20meV) between the electron pocket (BCB2) bottom at M and the valence band (BVB1) top near Γ (BVB1). This negative band gap clearly shows that the $TlBiTe_2$ is a semi-metal if E_F resides inside this region.

This semi-metalicity of $TlBiTe_2$ not only corrects the conventional misunderstanding of it as a narrow gap semiconductor[23, 27], but also naturally solves the mysterious puzzle on the small thermoelectric power of $TlBiTe_2$[22, 24]. Since electrons and holes have opposite signs for their thermoelectric power S, the co-existence of the conduction electron (near Γ) and hole (at M) pockets (due to the negative band gap between BCB2 and BVB1) results in a greatly reduced S because of the cancelation of their opposite contributions. As the thermoelectric figure of merit $ZT = S^2\sigma/\kappa T$ (where σ and κ are the electric and thermal conductivity, respectively), the greatly reduced S leads to even further suppressed ZT due to its quadratic dependence on S.

The band structure of $TlBiSe_2$, another compounds from the Tl-based ternary family, is summarized in Fig. 4(band structure near Γ) and Fig. 5 (broad k-space scans). Similar to $TlBiTe_2$, The existence of a single surface Dirac cone at the Γ point (with a velocity of $\sim 6.85 \times 10^5$m/s ,or 4.52eV·Å, slightly larger than that of $TlBiTe_2$) can be seen in both figures, confirming its topological non-triviality.

The main difference between $TlBiSe_2$ and $TlBiTe_2$ is that the Dirac point of $TlBiSe_2$ resides on the top of the BVB [Fig. 4(a,b)]; and the bulk energy gap at Γ [∼200meV, see Fig. 4(b)] is much larger than the energy scale of room temperature (26meV), making it a large gap topological insulator suitable for promising applications in low-power electronic and spintronic devices at room temperature. Compared to the previously found 3D topological insualtor family Bi_2Te_3/Bi_2Se_3

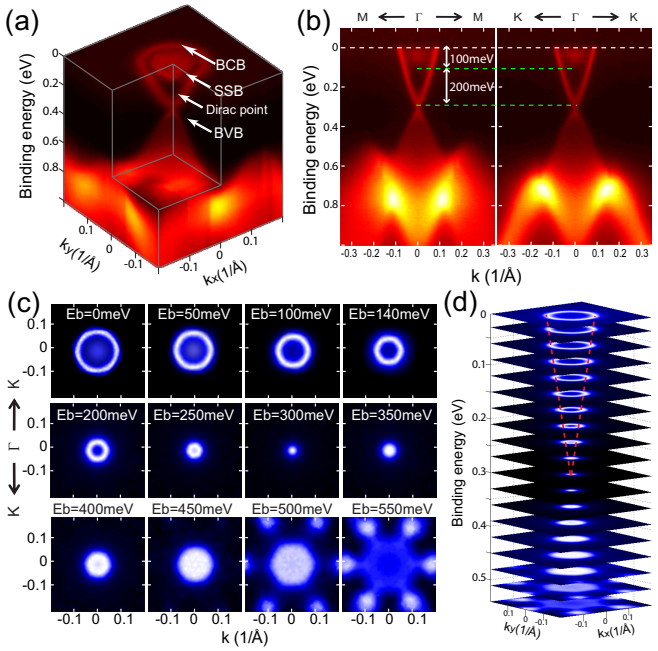

FIG. 4: (Color) (a) 3D illustration of the band structure of $TlBiSe_2$ around Γ, with the BCB, BVB, SSB and the Dirac point indicated. (b) Detailed band structure along M-Γ-M and K-Γ-K directions, with less anisotropy compared to Fig. 2(c). The bottom of the BCB at Γ is ∼100meV below E_F and the Dirac point residing on top of the BVB is ∼200meV below the BCB bottom. The smearing of the distinct SSB below the Dirac point is due to the hybridization with the BVB. (c) Constant energy contours of the band structure at different binding energies. (d) Stacking constant energy plots shows the evolution of the band structure. Red dashed line traces the dispersion of the SSB from the Dirac point.

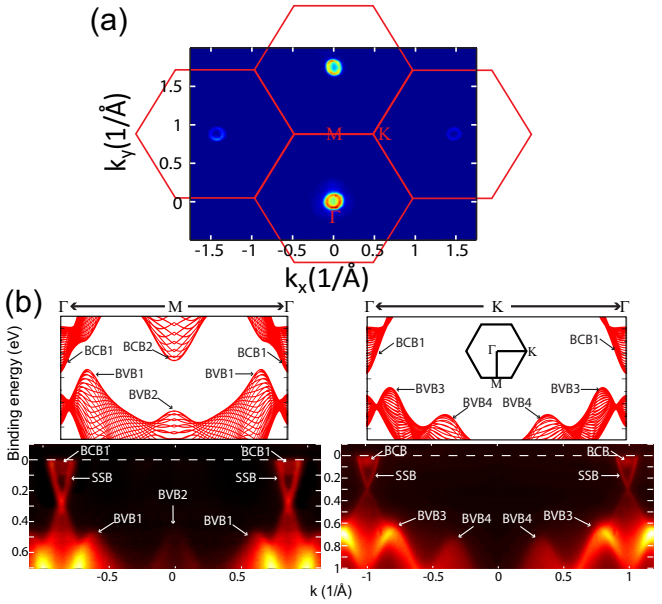

FIG. 5: (Color) (a) Broad FS map of n-type $TlBiSe_2$ shows a FS sheet without BCB pocket at M point. (b) Comparison between the calculation (top panels) and measured band structure (bottom panels). Results along $\Gamma - M - \Gamma$ and $\Gamma - K - \Gamma$ directions are shown on the left and right rows, respectively. Prominent BCB, BVB and SSB features are marked in both the calculated and measured band structures.

where the quintuple layer units are bonded by van de Waal's force[4], the much improved mechanical properties of $TlBiTe_2$ resulted from the covalence boding between atomic layers[14] make it more favorable for real world devices.

In addition, the bulk band structure of $TlBiSe_2$ is simpler around Γ and less anisotropic between Γ-M and Γ-K directions [Fig. 4(a,b)] compared to that of $TlBiTe_2$ [Fig. 2(a,c)]. This simplicity can also be seen in the constant energy contour plots [Fig. 4(c)] and its evolution [Fig. 4(d)]. Comparing Fig.4(c) to Fig. 2(b), we notice that the SSB FS of $TlBiSe_2$ is a convex hexagon, contrast to that of $TlBiTe_2$ which shows slightly concave geometry. This difference resembles the difference between the SSB FSs of Bi_2Te_3 and Bi_2Se_3, and can be reflected by different observations in experiments such as scanning tunneling microscopy/spectroscopy STM/STS[29, 30].

Besides the simpler band geometry around Γ, the broad range band structure(Fig. 5) of $TlBiSe_2$ is also less complicated without the electron pocket at M point, as shown in both the FS map (Fig. 5a) and the dispersions plots [Fig. 5(b), bottom row]. Also, although the comparison between the experiments and calculation [Fig. 5(b)] again shows general agreement, the BCB2 feature at M point in the calculation (top left panel) was not seen in the measurements (bottom left panel), causing the missing of an electron pocket at M point in Fig. 5(a).

In summary, the identification of the single Dirac cone surface state in both $TlBiTe_2/TlBiSe_2$ and the possibility of the topological superconducting phase in $TlBiTe_2$ extends the study of topological quantum phases to a new family of materials; and the better physical properties of these ternary chalcogenides make the realization of applications more realistic. Furthermore, our finding of the semi-metalicity in $TlBiTe_2$ solves the long standing puzzle on the unique thermoelectric properties of $TlBiTe_2$ in this family of high-temperature thermoelectric materials.

Acknowledgements We thank X. L. Qi and C.X. Liu for insightful discussions. This work is supported by the Department of Energy, Office of Basic Energy Science under contract DE-AC02-76SF00515.

[1] X. L. Qi and S. C. Zhang, Phys. Today 63, 33 (2010)
[2] A. Bernevig, T. L. Hughes and S. C. Zhang, Science 314, 1757 (2006)
[3] M. Konig et al., Science 318, 766 (2007)
[4] H. Zhang, et. al., Nature Phys. 5, 438 (2009)
[5] Y. Xia, et. al., Nature Phys. 5, 398 (2009)
[6] Y. L. Chen, et. al., Science 325 178 (2009)
[7] L. Fu, C. L. Kane, and E. J. Mele, Phys. Rev. Lett. 98, 106803 (2007)
[8] X. L. Qi, T. L. Hughes, and S. C. Zhang, Phys. Rev. B 78, 195424 (2008)
[9] J. E. Moore, and L. Balents, Phys. Rev. B 75, 121306(R) (2007)
[10] R. Roy, Phys. Rev. B 79, 195321 (2009)
[11] X. L. Qi, et. al., Phys. Rev. Lett. 102, 187001 (2009)
[12] L. Fu and E. Berg, arxiv:cond-mat/0912.3294 (2009)
[13] Y. S. Hor, et. al., arxiv:cond-mat/1006.0317 (2010)
[14] B. Yan, et. al., Euro. Phys. Lett. 90 37002 (2010)
[15] F. Wilzcek, Nature 458, 129 (2009)
[16] X. L. Qi, T. L. Hughes and S. C. Zhang, arxiv:cond-mat/0908.3550 (2009)
[17] A. P. Schnyder, et. al., Phys. Rev. B 78, 195125 (2008)
[18] F. Wilczek, Nature Phys 5, 614-618 (2009)
[19] C. Nayak, et. al., Rev. Mod. Phys. 80, 1083 (2008)
[20] H. Lin, et. al., arxiv:cond-mat/1003.2615 (2010)
[21] R. Hein and E. Swiggard, Phys. Rev. Lett. 24, 53-55 (1970)
[22] D. P. Spitzer and J. A. Kykes, J. Appl. Phys. 37 1563 (1966)
[23] K. chrissafis, et. al., Phys. Stat. Sol. (a) 196, 515 (2003)
[24] K. Kurosaki, A. Kosuga and S. Yamanaka, J. Alloys Comp. 351, 279 (2003)
[25] K. Kurosaki, et. al., J. Alloys Comp. 376, 43 (2004)
[26] K. F. Hsu, et. al., Science, 303, 818 (2004)
[27] K. Hoang and S. D. Mahanti, Phys. Rev. B 77, 205107 (2008)
[28] J. D. Jensen, et. al., Phys. Rev. B 6, 319 (1972)
[29] L. Fu, Phys. Rev. Lett. 103 266801 (2009)
[30] Z. Alpichshev, et. al., Phys. Rev. Lett. 104 016410 (2010)